第 44 卷 第 3 期
2023 年 3 月

焊 接 学 报
TRANSACTIONS OF THE CHINA WELDING INSTITUTION

Vol. 44(3):70 − 76
March 2023

基于自约束结构炸药的 T2/Q345 爆炸焊接及数值模拟

李雪交， 钱敬业， 毕志雄， 张廷赵， 代弦德， 荣凯
(安徽理工大学, 淮南, 232001)

摘要: 为提高炸药能量利用效率、降低能量耗散, 利用自约束结构炸药进行爆炸焊接研究. 以 T2 铜和 Q345 钢分别作为复层与基层, 自约束结构炸药作为焊接炸药, 借助 ANSYS/AUTODYN 软件模拟爆炸焊接过程, 并进行 T2/Q345 爆炸焊接试验, 对复合板试件进行拉剪性能检测和微观形貌观察分析其焊接质量. 结果表明, T2/Q345 爆炸焊接的碰撞速度距起爆端 100 mm 后均大于临界碰撞速度 345 m/s, 距起爆端 150 mm 处碰撞速度达到最大值 567 m/s. T2/Q345 复合板起爆端呈直线结合, 并随着传爆距离增加变为波形结合. T2/Q345 复合板远离起爆端的平均剪切强度为 237.0 MPa, 断裂位置位于铜一侧. 试件被拉剪破坏后的铜层出现加工硬化现象, 远离结合界面的显微硬度和塑性变形程度呈增强趋势. 自约束结构炸药可降低自身爆炸产物飞散, 使炸药能量更多地转化为复层动能, 提高能量利用率.

创新点: (1) 采用自约束结构炸药作为焊接炸药成功实现 T2/Q345 爆炸焊接, 并分析了复合板的微观形貌和力学性能.
(2) 运用 ANSYS/AUTODYN 软件模拟爆炸焊接过程, 分析自约束结构炸药降低能量耗散、提高能量利用效率原因.

关键词: 爆炸焊接; 自约束结构炸药; 数值模拟; 结合性能
中图分类号: TG 442 **文献标识码:** A **doi:** 10.12073/j.hjxb.20220419002

0 序言

爆炸焊接 (爆炸复合) 是一种复合材料的加工技术, 将炸药爆炸反应释放的化学能转化为焊接材料动能, 通过高速碰撞使界面间形成焊接接头[1]. 已成功实现数百种金属以及非金属的焊接, 被广泛应用于化工设备、船舶制造及航空航天等领域[2-4]. 炸药爆炸能量主要通过冲击波、爆热和爆炸产物动能等形式释放[5]. 爆炸产物会不受约束地从炸药上部飞散, 造成用于焊接的能量较低.

为提高能量利用效率、减少能量耗散, 国内外学者开展了大量研究. Lysak 等人[6] 提出了一种评估爆炸焊接效率的方法, 由炸药的化学能转化为焊接接头区域金属塑性变形所消耗的能量效率在 0.5% ~ 3% 之间. Yang 等人[7] 提出胶体水覆盖炸药, 通过改变胶体水厚度研究覆盖约束对爆炸焊接参数的影响. 相较于无覆盖炸药, 胶体水厚度为 15 ~ 45 mm 时, 碰撞速度可提高 38.9% 至 71.9%. Sun 等人[8] 采用闭合装药结构, 将 2 块复合板通过一次爆炸实现焊接, 从而提高炸药能量利用效率、节省焊接药量.

针对目前焊接炸药能量利用效率低的问题, 文中采用自约束结构装药进行爆炸焊接研究. 通过改变装药结构, 利用上层高爆速炸药爆轰约束下层低爆速炸药爆炸产物的飞散, 使炸药爆炸能量更多地转化为焊接能量, 提高能量利用率. 以两种不同爆速的乳化炸药叠放制成自约束结构炸药, 通过 ANSYS/AUTODYN 数值模拟, 与两单层结构炸药对比, 研究双层蜂窝结构炸药上层炸药对下层炸药产生的自约束效果. 采用自约束结构炸药进行 T2/Q345 爆炸焊接, 结合微观形貌观察与力学性能测试分析复合板的结合性能.

收稿日期: 2022 − 04 − 19
基金项目: 国家自然科学基金资助项目 (11872002); 安徽省自然科学基金资助项目 (1808085QA06); 安徽省博士后基金资助项目 (2019B355).

1　计算模型

1.1　自约束结构炸药

以乳化基质为基，中空玻璃微球作为敏化剂和稀释剂. 通过改变该稀释剂含量，制备微球含量分别为 15% 和 25% 的乳化炸药，其相应爆速为 3 512，2 505 m/s. 2 种炸药分别作为高爆速层和低爆速层，紧密贴合制备用于爆炸焊接的自约束结构炸药. 其利用高爆速层的爆炸为低爆速层的产物飞散提供约束，以此提高炸药能量利用率.

1.2　爆炸焊接几何模型

光滑粒子流体动力学方法 (SPH) 采用质点组来描述连续体的力学行为，可避免极度大变形时造成的网格畸变问题，被广泛应用到描述爆炸、射流等连续体的力学行为问题. SPH 法的粒子数量直接影响到数值模拟的精确性，但粒子数越多，其搜索算法越耗时[9].

考虑到模拟结果的精确性和双层炸药粒子多次碰撞计算的复杂性，使用 ANSYS/AUTODYN 2D 划分的粒子尺寸为 100 μm × 100 μm. 复板材料为 T2 铜，尺寸为 300 mm × 3 mm. 基板材料为 Q345 钢，尺寸为 300 mm × 15 mm，基复层间隙 5 mm. 自约束结构炸药的高爆速层和低爆速层尺寸均为 300 mm × 4 mm，自约束结构炸药模型及起爆点位置如图 1 所示.

图 1　计算模型
Fig. 1　Computational model

为对比模拟结果，将自约束结构炸药的高爆速层和低爆速层分别单独作为焊接炸药，建立 2 组单层炸药模型. 两模型炸药尺寸为 300 mm × 8 mm，其余模型参数不变.

1.3　材料模型和状态方程

乳化炸药选用 Jones-Wilkins-Lee(JWL) 状态方程 (EOS)，其计算式为[10]

$$P = A_{\mathrm{J}}\left(1-\frac{\omega}{R_1 V}\right)e^{-R_1 V} + B_{\mathrm{J}}\left(1-\frac{\omega}{R_2 V}\right)e^{-R_2 V} + \frac{\omega E_0}{V} \tag{1}$$

式中：P 为爆轰产物压力；A_{J}, B_{J}, R_1, R_2 和 ω 为材料常数；E_0 为初始比内能；V 为爆轰气体产物的相对比容. 自约束结构炸药的高爆速层和低爆速层具体 JWL 状态参数见表 1[3, 5].

表 1　炸药的 JWL 状态参数
Table 1　JWL EOS parameters of explosive

材料	材料常数A_{J}/GPa	材料常数B_{J}/GPa	材料常数R_1	材料常数R_2	材料常数ω
高爆速层	31.7	0.223	8.52	2.30	0.22
低爆速层	11.2	0.108	9.12	2.46	0.22

基复板选用 Johnson-Cook 材料模型[11]，其计算式为

$$\sigma = \left(A + B\varepsilon_{\mathrm{p}}^{n}\right)\left(1 + C\ln\dot{\varepsilon}_{\mathrm{p}}^{*}\right)\left(1 - T^{*m}\right) \tag{2}$$

$$T^{*} = (T - T_{\mathrm{r}})/(T_{\mathrm{m}} - T_{\mathrm{r}}) \tag{3}$$

式中：ε_{p} 为材料的有效塑性应变；$\dot{\varepsilon}_{\mathrm{p}}^{*}$为材料的有效塑性应变率；$A$, B, C, m 和 n 为材料的相关常数；T^{*}为材料的无量纲温度；T_{r} 为室温；T_{m} 为材料的熔点. T2 铜和 Q345 钢的 Johnson-Cook 材料模型参数见表 2[3, 5].

表 2　T2 铜和 Q345 钢的 Johnson-Cook 材料模型参数
Table 2　Johnson-Cook model parameters of T2 copper and Q345 steel

材料	屈服应力A/GPa	硬化模量B/GPa	硬化指数n	应变率强化参数C	软化指数m	金属熔点T_{m}/K	室温T_{r}/K
T2铜	0.09	0.292	0.31	0.025	1.09	1 356	294
Q345钢	0.79	0.51	0.26	0.014	1.03	1 793	294

1.4　碰撞速度

炸药对复板的作用主要表现为碰撞速度，其是影响焊接效果的重要参数. 低于临界碰撞速度，复合界面会因焊接能量较小无法焊接合，高于极限碰撞速

度易导致界面因过熔化造成脱焊，通常位于两者之间焊接质量较好.

异种金属临界碰撞速度 $v_{p,min}$ 可由下式计算[3]

$$v_{p,min}=\begin{cases} v_{p1}\left(\dfrac{C_{V1}\rho_1+C_{V2}\rho_2}{C_1\rho_1C_2\rho_2}\right) & p_1>p_2 \\ v_{p2}\left(\dfrac{C_{V1}\rho_1+C_{V2}\rho_2}{C_{V1}\rho_1C_{V2}\rho_2}\right) & p_2>p_1 \end{cases} \tag{4}$$

$$v_{p1}=\sqrt{\frac{\sigma_{b1}}{\rho_1}},\quad v_{p2}=\sqrt{\frac{\sigma_{b2}}{\rho_2}} \tag{5}$$

$$p_1=\frac{C_{V1}\rho_1v_{p1}}{2},p_2=\frac{C_{V2}\rho_2v_{p2}}{2} \tag{6}$$

式中：v_{p1} 和 v_{p2} 分别是基层材料之间和复层材料之间的最小碰撞速度；p_1 和 p_2 是基层材料之间和复层材料之间的碰撞压力；C_{V1} 和 C_{V2} 分别是基复层的体积声速；ρ_1 和 ρ_2 分别是基复层的密度；σ_{b1} 和 σ_{b2} 是基复层的抗拉强度.

李晓杰[12] 提出基复层最大碰撞速度 $v_{p,max}$ 可表示为

$$v_{p,max}=\frac{2\sqrt[4]{t_{min}/\pi}}{v_{c,min}}\sqrt{\rho_1C_{p1}\sqrt{\alpha_1}+\rho_2C_{p2}\sqrt{\alpha_2}}\sqrt{\frac{T_{mpmin}C_{V1}^2C_{V2}^2}{N\left(C_{V1}^2+C_{V2}^2\right)}}\sqrt{\frac{\rho_1\delta_1+\rho_2\delta_2}{\rho_1\delta_1\rho_2\delta_2}} \tag{7}$$

式中：C_{p1} 和 C_{p2} 分别是基复层的比热容；α_1 和 α_2 分别是基复层的热扩散率；δ_1 和 δ_2 分别是基复层的厚度；T_{mpmin} 是基复层材料中较低的熔点；t_{min} 是反射稀疏波到复合界面的最短时间；$v_{c,min}$ 是基复层之间的临界碰撞点移动速度；N 是与基复层材料体积声速有关的系数.

2 爆炸焊接试验

爆炸焊接采用的复层和基层分别为 T2 铜和 Q345 钢，其尺寸为 300 mm × 150 mm × (15 + 3) mm. 基复层的力学性能参数见表 3.

表 3 基复层的力学性能参数

Table 3 Physical and mechanical properties of flyer and base plates

材料	熔点T_m/°C	硬度H/HV	屈服强度R_{eL}/MPa	抗拉强度R_m/MPa	体积声速C/(m·s^{-1})
T2铜	1 083	65	185	295	4 700
Q345钢	1 523	135	345	515	5 900

以乳化基质 (其组分见表 4) 为基，通过改变微球含量，制备 2 种不同爆速的乳化炸药. 壁厚 60 μm、六边形单元边长 8 mm、高度 4 mm 的蜂窝铝板材作为装药药框，将两种乳化炸药分别填入蜂窝板孔隙中，分别作为具有自约束功能炸药的低爆速层与高爆速层，如图 2 所示. 蜂窝铝板材具有良好的竖向抗压性，可保证装药厚度均匀. 将高爆速层叠放于低爆速层上方，制备用于爆炸焊接的 8 mm 厚度自约束结构炸药.

表 4 乳化基质组成 (质量分数，%)

Table 4 Emulsion matrix component

NH_4NO_3	$NaNO_3$	H_2O	$C_{18}H_{38}$	$C_{24}H_{44}O_6$
71	11.5	11	3.7	2.8

将 T2 铜板和 Q345 钢板内表面打磨抛光，放置在爆炸球罐基础上. 在复层表面涂抹一层黄油避免被高温灼伤，再将自约束结构炸药作为焊接炸药放置于复板表面. 爆炸焊接装置采用平行安装结构，如图 3 所示. T2/Q345 爆炸焊接后对 T2/Q345 复合板进行力学性能检测和微观形貌观察.

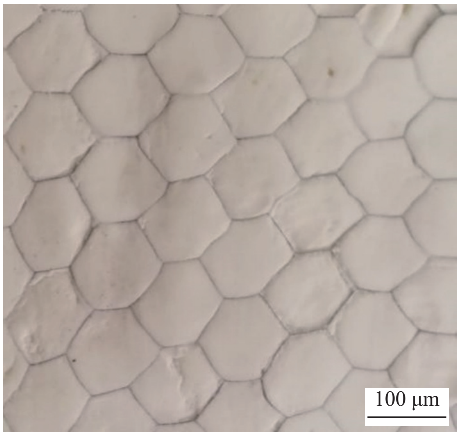

图 2 蜂窝结构炸药

Fig. 2 Honeycomb structure explosive

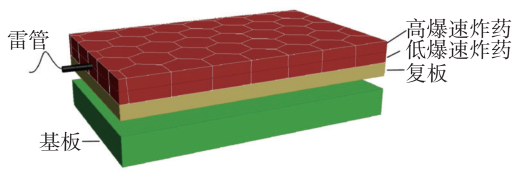

图 3 爆炸焊接装配图

Fig. 3 Assembly drawing of explosive welding

3　结果与讨论

3.1　数值模拟分析

通过自约束结构炸药进行 T2/Q345 爆炸焊接数值模拟, 分析提高能量利用效率和减少爆炸焊接药量原因. 自约束结构炸药由高爆速层和低爆速层组成, 总装药厚度为 8 mm.

为对比效果, 将同样 8 mm 厚度的高爆速炸药和低爆速炸药分别建立计算模型. 输出 3 个模型的模拟结果, 如图 4 所示.

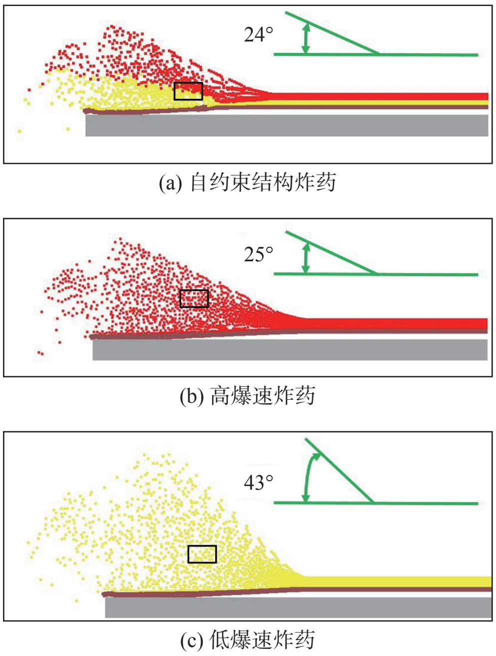

(a) 自约束结构炸药

(b) 高爆速炸药

(c) 低爆速炸药

图 4　3 种装药结构的模拟结果

Fig. 4　Simulation results of three kinds of explosives. (a) self-restraint structure explosive; (b) high detonation velocity explosive; (c) low detonation velocity explosive

由图 4 可知, 自约束结构炸药爆炸产物的侧向飞散角为 24°, 小于高爆速炸药的 25°和低爆速炸药的 43°. 炸药爆炸产物在稀疏波的作用下发生侧向飞散, 其一部分碰撞复板, 另一部分飞散到环境中. 通常, 炸药爆速越高, 其爆炸速度与产物飞散速度差距越大, 飞散角越小[13]. 爆速稳定时, 炸药的飞散角一般不变.

图 4 方框位置的爆炸产物粒子速度场如图 5 所示. 自约束结构炸药高爆速层的爆炸产物自由飞散, 其速度矢量均匀向上, 飞散角与单独的高爆速层相近. 但自约束结构炸药低爆速层爆炸产物的飞散受到高爆速层爆炸的约束影响, 速度矢量较为杂乱, 其飞散角远小于单独的低爆速层. 自约束结构炸药可以约束自身低爆速层爆炸产物的飞散, 可以使爆炸能量更多地转化为复板动能, 提高焊接炸药的能量利用率.

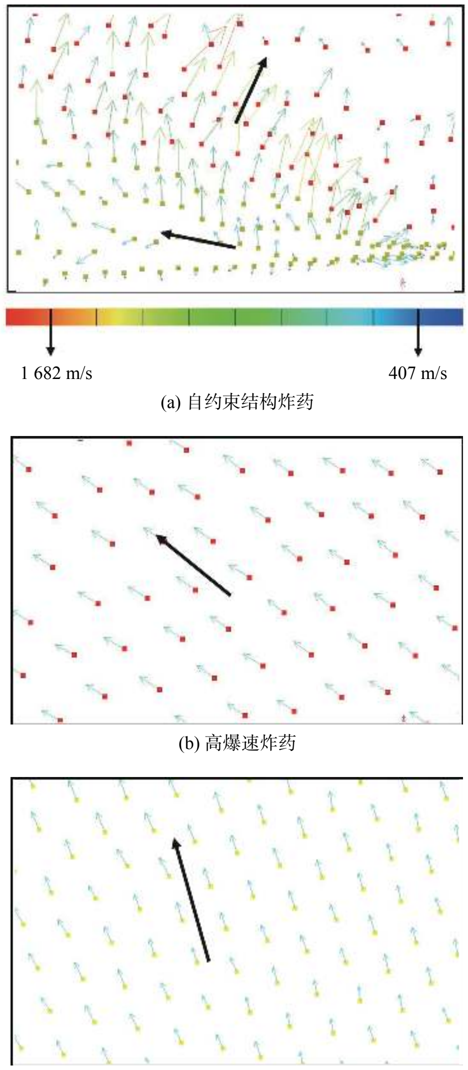

(a) 自约束结构炸药

(b) 高爆速炸药

(c) 低爆速炸药

图 5　3 种装药结构的粒子速度

Fig. 5　Particle velocity of three kinds of explosives. (a) self-restraint structure explosive; (b) high detonation velocity explosive; (c) low detonation velocity explosive

为便于分析爆炸焊接过程中碰撞速度的变化规律, 在 3 个模型的复层焊接面间隔 25 mm 选取 11 个关键点, 如图 6 所示. 将表 3 中的基复层材料参数代入式 (4) ~ 式 (7), 得到 T2/Q345 复合板的临

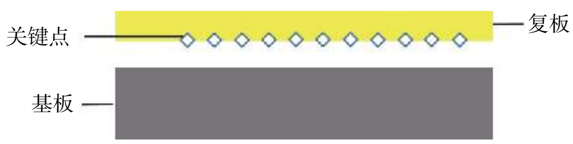

图 6　关键点取样示意图

Fig. 6　Schematic diagram of key point sampling

界碰撞速度 345 m/s 和极限碰撞速度 722 m/s.

通过模拟得到 3 个碰撞模型的 11 个关键点的碰撞速度. 虚线和实线分别代表 T2/Q345 爆炸焊接的临界碰撞速度和极限碰撞速度, 如图 7 所示.

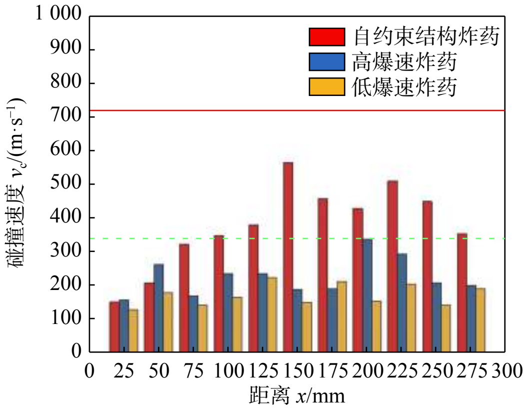

图 7 关键点碰撞速度

Fig. 7 Collision velocity of key points

由图 7 可知, 在距起爆端 50 mm 以内时, 自约束结构炸药的碰撞速度介于单独的高爆速炸药和低爆速炸药碰撞速度之间. 因为距起爆点较近时, 自约束结构炸药的高爆速层和低爆速层爆速均较低, 还未形成足够的自约束效果. 在距起爆端 75 mm 之后, 其碰撞速度远大于单独的高爆速炸药和低爆速炸药. 这是因为自约束炸药的高爆速层爆轰对下层低爆速层爆炸产物的飞散提供了约束, 使得低爆速层的炸药能量更多地转化为复层动能.

单独的高爆速炸药和低爆速炸药的碰撞速度在整个焊接过程中较为稳定, 最高碰撞速度分别为 338, 231 m/s, 均未达到临界碰撞速度 345 m/s, 位于 T2/Q345 爆炸焊接窗口之外, 难以获得良好的焊接效果. 而对于自约束结构炸药, 其碰撞速度随着传播距离增加逐渐加快, 距起爆端 100 mm 之后均大于临界碰撞速度, 在距起爆端 150 mm 处达到最大值 567 m/s, 此处的碰撞速度相较于单独的高爆速炸药和低爆速炸药分别提高了 185% 和 275%. 自约束结构炸药通过上部高爆速层的爆炸对低爆速层爆炸产物产生约束效果, 提高了炸药爆炸能量利用效率, 在降低焊接药量的同时, 为 T2/Q345 复合板获得良好结合质量提供了足够的碰撞能量.

3.2 微观形貌观察

采用自约束结构炸药进行 T2/Q345 爆炸焊接后, 为观察复合板界面结合状态, 沿爆轰方向切割试块, 分别距起爆端 50 mm 和 150 mm, 其微观形貌如图 8 所示.

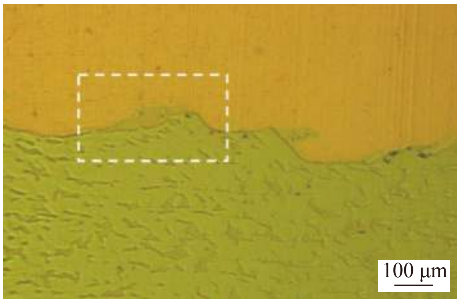

(a) 距起爆端 50 mm 处微观形貌

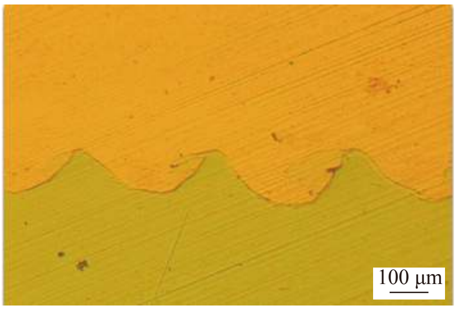

(b) 距起爆端 150 mm 处微观形貌

图 8 T2/Q345 复合板界面微观形貌

Fig. 8 Microstructures at the interface of T2/Q345 clad plate. (a) close to initiation end of 50 mm; (b) away from initiation end of 150 mm

图 8a 为 T2/Q345 复合板距起爆端 50 mm 处结合界面微观形貌, 界面呈平直状. 数值模拟结果显示此处的碰撞速度为 209 m/s, 低于 T2/Q345 复合板的临界碰撞速度 345 m/s, 未产生明显的熔化层, 但是局部区域会出现熔化块 (见图 8a 中白色虚线区域). 界面金属在绝热压缩和塑性变形热的共同作用下产生强烈的热效应, 导致界面出现熔化现象. 过度熔化会影响复合板界面的结合质量, 但厚度较薄的熔化有利于增大界面结合强度.

图 8b 为 T2/Q345 复合板距起爆端 150 mm 处界面的微观形貌, 其平均波长 250 μm、波幅 100 μm. 数值模拟结果显示此处的碰撞速度为 567 m/s, 高于其临界碰撞速度 345 m/s, 复合界面呈波形结合.

爆炸焊接界面主要有平直状和波状 2 种, 其中波状界面因结合面积更大而具有更高的结合性能[14]. 根据 Bahrani 等人[15] 提出的复板流侵彻机理, 当基复层间的碰撞压力超过动态屈服强度极限时, 会使金属形成不可压缩且无粘性的射流. 金属射流在基层上产生的压陷作用导致界面产生波谷, 同时被移走基层材料堆积形成波峰, 从而形成波形界面. 随着传爆距离增加, 自约束结构炸药迅速转为稳定爆炸, 爆炸能量转化为基层碰撞动能的效率也在提高, 所以 T2/Q345 结合界面从起始的平直状结合变为稳定的波状结合.

3.3　力学性能检测

为测试 T2/Q345 爆炸复合板的结合质量，采用室温拉剪试验进行力学性能检测. 拉剪试件结合面积为 25 mm × 3.8 mm，结构示意图如图 9 所示. 图 10 为 T2/Q345 复合板的应力–位移曲线，T2/Q345 复合板的平均最大拉伸力为 22.5 kN，剪切强度为 237.0 MPa. 拉剪破坏实物如图 11 所示，可以看出断裂发生在铜侧区域，且该侧发生极大塑性变形导致拉伸破坏，表明 T2/Q345 复合板界面结合强度较好.

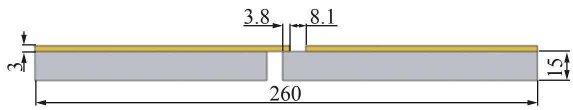

图 9　拉剪试件示意图 (mm)

Fig. 9　Schematic diagram of tensile-shear specimen

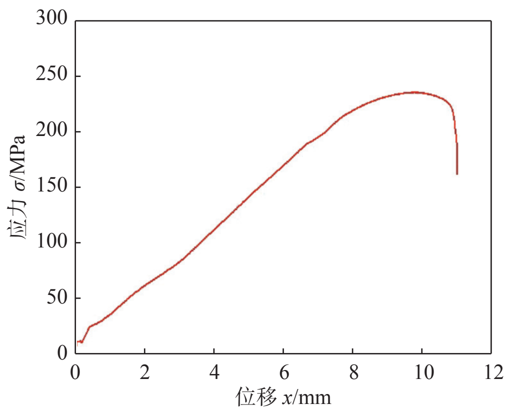

图 10　拉剪试验应力–位移曲线

Fig. 10　Stress-displacement curve of tensile-shear test

为分析拉剪试件破坏后塑性变形程度，进行显微硬度分析 (测试位置见图 11 实线)，试件拉剪前后铜侧硬度变化如图 12 所示. 在距结合面较近时，拉剪试件破坏后铜侧硬度变化不大，说明其塑性变形程度较低. 随着与焊接面距离的增加，剪切破坏前试件的硬度逐渐下降，但破坏后试件的硬度剧烈增大. 说明试件在拉剪过程中发生了较大塑性变形，产生加工硬化，导致显微硬度上升.

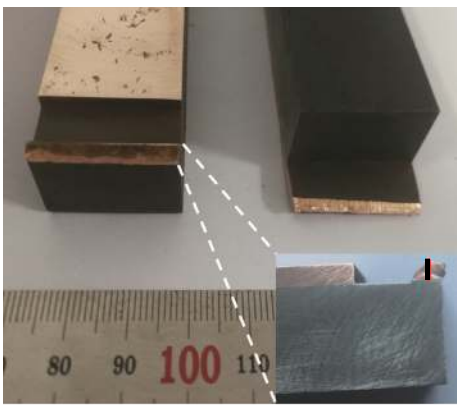

图 11　拉剪试件破坏实物图

Fig. 11　Physical image of tensile-shear failure specimen

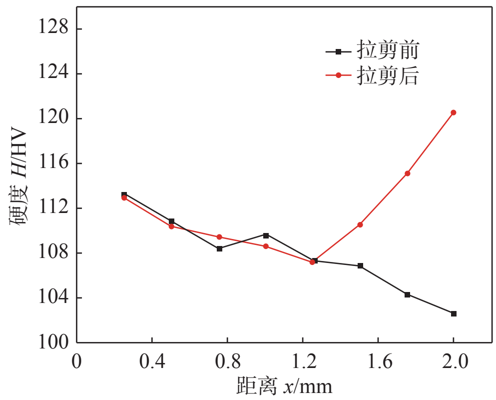

图 12　破坏前后硬度变化对比

Fig. 12　Comparison of hardness changes before and after failure

4　结论

(1)T2/Q345 爆炸焊接数值模拟显示自约束结构炸药的爆炸产物侧向飞散角为 24°，小于高爆速炸药的 25°和低爆速炸药的 43°. 自约束结构炸药可以约束自身低爆速层的爆炸产物飞散，使爆炸能量更多地转化为复板动能，提高了焊接炸药的能量利用率.

(2) 距起爆点较近时炸药爆速较低，自约束效果不明显，但在距离起爆端 75 mm 后，上部的高爆速层爆轰对下部的低爆速层爆炸产物的飞散提供了足够的约束，使得下部的低爆速层炸药能量更好地转化为复板动能.

(3) 自约束结构炸药进行 T2/Q345 爆炸焊接的碰撞速度在距起爆端 150 mm 处达到最大值 567 m/s，此处的碰撞速度相较于单独的高爆速炸药和低爆速炸药分别提高 185% 和 275%. 随着炸药传播距离增加，T2/Q345 复合板界面由直线结合变为波形结合.

(4) 拉剪试件破坏前，距离界面越远，铜的显微硬度越小. 而试件在拉剪破坏后，距离界面越远，塑性变形越大，加工硬化增大，使得铜的显微硬度增加. 而且 T2/Q345 复合板拉剪强度为 237.0 MPa，破坏位置位于铜一侧，表明 T2/Q345 界面具有良好

的结合强度.

参考文献

[1] Jiang C, Long W M, Feng J, *et al*. Thermal fatigue behavior of copper/stainless steel explosive welding joint[J]. China Welding, 2021, 30(4): 25 − 29.

[2] 毕志雄, 李雪交, 吴勇, 等. 钛箔/钢爆炸焊接的界面结合性能 [J]. 焊接学报, 2022, 43(4): 81 − 85.
Bi Zhixiong, Li Xuejiao, Wu Yong, *et al*. Interfacial bonding properties of titanium foil/steel explosive welding[J]. Transactions of the China Welding Institution, 2022, 43(4): 81 − 85.

[3] 毕志雄, 李雪交, 吴勇, 等. 自约束结构装药下 T2/Q345 爆炸焊接研究 [J]. 含能材料, 2021, 29(5): 394 − 398.
Bi Zhixiong, Li Xuejiao, Wu Yong, *et al*. Study on explosion welding of T2/Q345 alloys with self-restraint explosive[J]. Chinese Journal of Energetic Materials, 2021, 29(5): 394 − 398.

[4] 田启超, 马宏昊, 沈兆武, 等. $Al_{0.1}$CoCrFeNi 高熵合金/TA2 钛复合板爆炸焊接试验及性能测试 [J]. 焊接学报, 2021, 42(6): 22 − 29.
Tian Qichao, Ma Honghao, Shen Zhaowu, *et al*. Explosive welding and performance test of $Al_{0.1}$CoCrFeNi high-entropy alloy/TA2 composite plate[J]. Transactions of the China Welding Institution, 2021, 42(6): 22 − 29.

[5] 郑远谋. 爆炸焊接和爆炸复合材料 [M]. 北京: 国防工业出版社, 2017.
Zheng Yuanmou. Explosive welding and explosive composite material[M]. Beijing: Natianal Defense Industry Press, 2017.

[6] Lysak V L, Kuzmin S V. Energy balance during explosive welding[J]. Journal of Materials Processing Technology, 2015, 222: 356 − 364.

[7] Yang M, Ma H H, Shen Z W. Study on the effects of explosive covering on explosive welding of stainless steel to steel[J]. Propellants Explosives Pyrotechnics, 2019, 44: 609 − 616.

[8] Sun Z R, Shi C G, Shi H, *et al*. Comparative study of energy distribution and interface morphology in parallel and double vertical explosive welding by numerical simulations and experiments[J]. Materials and Design, 2020, 195: 109027.

[9] 曾翔宇, 李晓杰, 曹景祥, 等. 材料强度对爆炸焊接结合界面的影响 [J]. 爆炸与冲击, 2019, 39(5): 139 − 145.
Zeng Xiangyu, Li Xiaojie, Cao Jingxiang, *et al*. Interface characteristics of explosive welding for different strength plates[J]. Explosion and Shock Waves, 2019, 39(5): 139 − 145.

[10] Sandra P, Marc G, Alexandre L, *et al*. Investigation of JWL equation of state for detonation products at low pressure with radio interferometry[J]. Propellants Explosives Pyrotechnics, 2018, 43: 1157 − 1163.

[11] Daridon L, Oussouaddi O, Ahzi S. Influence of the material constitutive models on the adiabatic shear band spacing: MTS, power law and Johnson-Cook models[J]. International Journal of Solids and Structures, 2004, 41: 3109 − 3124.

[12] 李晓杰. 双金属爆炸焊接上限 [J]. 爆炸与冲击, 1991, 4(2): 134 − 138.
Li Xiaojie. The upper limit of bimetal explosive welding parameters[J]. Explosion and Shock Waves, 1991, 4(2): 134 − 138.

[13] 邵丙璜, 张凯. 爆炸焊接原理及其工程应用 [M]. 大连: 大连理工大学出版社, 1987.
Shao Binhuang, Zhang Kai. Principles and engineering applications of explosive welding[M]. Dalian: Dalian University of Technology Press, 1987.

[14] 陈代果, 姚勇, 邓勇军, 等. 炸药覆盖层厚度对爆炸焊接的影响 [J]. 火炸药学报, 2019, 42(1): 52 − 57.
Chen Daiguo, Yao Yong, Deng Yongjun, *et al*. Effects of covering thickness of explosives on explosive welding[J]. Chinese Journal of Explosives & Propellants, 2019, 42(1): 52 − 57.

[15] Bahrani A S, Black T J, Crossland B. The mechanics of wave formation in explosive welding[J]. Mathematical and Physical Sciences, 1967, 296(1445): 123 − 136.

第一作者:李雪交，博士，副教授；主要从事含能材料开发与应用；Email: xjli@aust.edu.cn.

（编辑： 高忠梅）

anism is mainly the brittle fracture of WC particles and the lamellar tearing along the WC-W_2C interface.

Highlights: (1) The microstructure evolution of the interfacial reaction layer of WC/TC4 composite with different contents prepared by SLM was studied.
(2) The synergistic effect of air flow, heat and metal powder in molten pool and the growth mechanism of grain epitaxial reaction at particle/matrix interface during processing were expounded.
(3) The fracture mechanism of WC/TC4 composites and the strengthening effect of particle/matrix interface are expounded.

Key words: laser selective melting; WC/TC4 composites; interface; fracture mechanism

Analysis of interaction mechanism between feeding flux sheet and arc in ultra-narrow gap welding TANG Guoxi[1], ZHU Liang[1], ZHANG Aihua[2], ZHOU Hui[1], GUO Ning[1], ZHOU Yi[1](1. State Key Laboratory of Advanced Processing and Recycling Non-ferrous Metals, Lanzhou University of Technology, Lanzhou 730050, China; 2. Lanzhou University of Technology, Lanzhou 730050, China). pp 54-60

Abstract: In the ultra-narrow gap welding of the fed-in flux sheet constrained arc, the interaction between the continuously fed flux sheet and the arc affected the stability of the welding process. A method of rapidly interrupting the arc was used to obtain the shape of the molten pool and the instantaneous melting morphology of the flux sheet at the arc-extinguishing position . The relationship between the action length of the flux sheet on the arc and the degree of arc confinement was analyzed. The results showed that the feeding speed of the flux sheet was increased or the welding voltage was reduced , which could make the action length of the flux sheet on the arc increase. When it increased to a certain extent, the arc was effectively constrained at the bottom of the groove to uniformly heat the root of the side wall, and the flat weld with good root fusion was obtained. When the degree of restraint was weakened, the arc heating area was concentrated on the two side walls, and it was too difficult to form an effective molten pool at the root of the groove. Finally a hole weld was formed.

Highlights: (1) A method of ultra-narrow gap welding with feed-in flux sheet confinement arc was established, and the 30 mm thick plates were ultra-narrow gap welded by multi-layer single-pass.
(2) The interaction mechanism between flux sheet and arc in ultra-narrow gap welding with confinement arc of flux sheet was revealed.

Key words: ultra-narrow gap welding; flux sheet confinement arc; process parameters; arc confinement degree

Study on microstructure and properties of laser flux-cored wire joint of titanium alloy FANG Naiwen, HUANG Ruisheng, WU Pengbo, MA Yiming, SUN Laibo, CAO Hao, ZOU Jipeng(Harbin Welding Institute Limited Company, Harbin 150028, China). pp 61-69

Abstract: The welding of TC4 titanium alloy plate was carried out by means of laser welding with filler wire and self-developed flux-cored wire, and the obtained welding joint was treated with 850 ℃ heat preservation for 2 hours and then cooled and annealed with furnace, the microstructure and mechanical properties of the welded joint were compared with those of the welded joint. The results showed that the welded joint was composed of α_p phase, α_s phase and β phase, the α' martensite structure was not found in the as-welded joint, the strength of the as-welded joint decreased, but the elongation and impact toughness at room temperature increased, and the tensile fracture of the as-welded joint was surrounded by a large number of tearing lips, the dimples are deep and uniform, showing microporous polymerized ductile fracture. It was found by XRD that the as-welded joint was mainly composed of α' martensite, and a few weak multi-angle α phase diffraction peaks were observed, and the central angle of α phase diffraction peaks in the heat-treated joint was the same as that in the as-welded joint, in addition, a rather sharp diffraction peak of β phase (110) was found.

Highlights: (1) The effect of heat treatment on the microstructure and mechanical properties of titanium alloy welded joints by laser wire-filler metal was studied.
(2) It is found that the presence of residual β phase in α_p/α_s interface can effectively guarantee the plasticity and toughness of the welded seam.

Key words: titanium alloy; laser filler wire welding; microstructure and properties

Explosive welding and numerical simulation of T2/Q345 clad plate based on self-restraint structure explosive LI Xuejiao, QIAN Jingye, BI Zhixiong, ZHANG Tingzhao, DAI Xiande, RONG Kai(Anhui University of Science and Technology, Huainan 232001,China). pp 70-76

Abstract: In order to improve the energy utilization rate and reduce the energy dissipation, explosive welding was carried out with self-restraint structure explosive. T2 copper and Q345 steel were used as fly and base layers, respectively, and self-restraint structure explosive was adopted as welding explosive. The explosive welding process was simulated by ANSYS/AUTODYN code, and the copper/steel explosive welded clad plate was prepared. The welding quality was analyzed by mechanical property testing and microscopic morphology observation. The results show that self- restraint structure could reduce the dissipation of its own detonation products, which makes more explosive energy into kinetic energy of flyer layer and improves energy utilization rate. The collision velocity of copper/steel explosive welding is greater than the critical collision velocity of 345 m/s after detonation distance is greater than 100 mm away from the initiation end. The ultimate collision velocity at a detonation distance of 150 mm is 567 m/s. The initiation end of the copper/steel clad plate is of linear bonding, the bonding interface is transformed into wavy bonding as detonation distance increases. The shear strength of copper/steel clad plate is 237. 0 MPa, and the fracture position is on the copper side. Copper layer existed work hardening after tension shear failure, and the farther measuring point from the interface is, the stronger the microhardness and plastic deformation is.

Highlights: (1) The explosive welding of copper/steel was successfully realized by using self-restraint structure explosive as welding explosive, and the microstructure and mechanical properties of composite plate were analyzed.
(2) Explosive welding process was simulated by ANSYS/AUTODYN code, and the reason that self-restraint structure explosive could reduce energy dissipation and improve utilization efficiency was analyzed.

Key words: explosive welding; self- restraint structure explosive; numerical simulation; welding quality

Effect of welding time and temperature on properties of Sn35Bi0.3Ag/Cu welded joints SHEN Bingwei, XU Mingyue, YANG Shangrong, LIU Guohua, XIE Ming, DUAN Yunzhao(Kunming Insitute of Precious Metals, State Key Laboratory of Advanced Technologies for Comprehensive Utilization of Platinum Metals, Sino-Platinum Metals Co., Ltd., Kunming 650106, China). pp 77-86

Abstract: Sn35Bi0. 3Ag/Cu welded joints were prepared at different welding time and temperature. The effects of welding time (1 ~ 9 min) and welding temperature (210 ~ 290 ℃) on the microstructure and mechanical properties of Sn35Bi0. 3Ag/Cu welded joints were studied by means of scanning electron microscope (SEM), universal tensile testing machine and ultrasonic scan machine. The results show that the Cu element diffuses into the welding interface and forms the (Cu_5Sn_6, Cu_3Sn) interface layer. The Ag_3Sn phase can inhibit the growth of interfacial layer. With the increase of welding time or welding temperature, the reaction layer thickens and the shear strength increases first and then decreases. The analysis of the fracture morphology of the welded joint shows that the fracture of the welded joint is jointly affected by Bi phase particles and Cu_6Sn_5 particles. The fracture of the welded joint occurs on the IMC / solder side. Bi phase particles and Cu_6Sn_5 particles affect the shear strength of the joint. In addition, when the welding time is 3 min and the welding temperature is 230 ℃, the brazing rate is the highest (99. 14%) and the shear strength reaches the maximum value (51. 8 MPa).

Highlights: (1) The effects of welding time and welding temperature on the interfacial reaction and mechanical properties of Sn35Bi0. 3Ag / Cu welded joints were studied.
(2) The defects of welded joints were evaluated and analyzed by ultrasonic nondestructive testing equipment.
(3) By analyzing the fracture morphology of the welded joint and combining the brazing rate and shear strengthof the joint, the optimal welding parameters are determined.

Key words: technological parameters; Sn35Bi0. 3Ag/Cu welded joint; shear strength; the brazing rate

Effect of Ti and Nb on microstructure and properties of Fe based surfacing alloy JIA Hua[1], GAO Ming[1], LIU Zhengjun[2](1. Dalian Ocean University, Dalian 116023, China; 2. Shenyang University of Technology, Shenyang 110870, China). pp 87-91

Abstract: Fe-Cr-C-B Fe based surfacing alloy was prepared by changing the addition of Ti or Nb. The microstructure and properties of surfacing alloy were tested and analyzed by means of scanning electron microscope, X-ray diffraction, Rockwell hardness tester and wear tester. The results show that in the surfacing alloy containing Ti or Nb, the primary austenite grain is refined, the eutectic structure is evenly distributed in a broken network, and black circular or massive TiC and rhombic or triangular NbC hard phase particles are formed re-